

A Nano- to Macroscale Tribological Study of PFTS and TCP Lubricants for Si MEMS Applications

Brendan P. Miller · Nimel D. Theodore ·
Matthew J. Brukman · Kathryn J. Wahl ·
Jacqueline Krim

Received: 22 July 2009 / Accepted: 29 December 2009 / Published online: 23 January 2010
© Springer Science+Business Media, LLC 2010

Abstract The reliability and lifetime of cyclic contacting Si MEMS is limited by adhesion and their tribological performance. In this study, the tribological effects of adding a lubricant (tricresyl phosphate, TCP) to a bound self-assembled monolayer (perfluorodecyltrichlorosilane, PFTS) at different length scales were examined using a quartz crystal microbalance (QCM), an atomic force microscope (AFM), a reciprocating microtribometer, and a macroscopic reciprocating tribometer. The results showed that the addition of TCP to a PFTS layer increased the number of cycles possessing low friction and wear by at least a factor of four in the macroscopic tribometer. Differences in friction response over the range of experimental scales were correlated to contact size and pressure. QCM measurements of TCP on PFTS showed a non-zero slip time, which suggests favorable tribological performance in larger length-scale regimes. This non-zero slip time also may indicate TCP mobility.

Keywords Nanotribology · MEMS devices · AFM · Silicon · Vapor phase lubricants

1 Introduction

MicroElectroMechanical Systems (MEMS) have the potential to revolutionize widespread technologies, but friction and other tribological issues are currently preventing commercialization of devices that contain surfaces in sliding contact [1–4]. Self-assembled monolayers (SAMs), while highly effective against release related stiction [5], have proven ineffective as MEMS lubricants [6]. Indeed, even the most robust SAMs fail to protect devices from tribological failure for either normal (tapping) contact or sliding (shear) contact [6]. Alternative MEMS lubrication schemes must therefore be developed if progress is to occur.

Eapen et al. [7] suggested that the addition of a mobile lubricant in combination with a bound chemisorbed SAM should decrease friction and wear over a longer period of time than either the bound SAM or mobile lubricants alone. In that study, the mobile lubricants were delivered to the device surface by liquid immersion. Others have also considered two-layer systems to improve tribological performance using similar deposition methods (solution casting, dip coating, and spin coating) [8–12]. Since capillary forces resulting from liquid immersion routinely cause stiction, a well-known source of failure in MEMS systems [13], this deposition process will not be viable for a wide range of MEMS devices.

One way to prevent capillary bridge formation during lubricant delivery is through vapor phase lubrication such as that proposed by Abdelmaksoud and Krim in 1998 [14]. Recently, studies of MEMS lifetime have been reported for adsorbed water over a full range of humidities [15]. Only adsorbed water layers that formed between 30 and 50% relative humidity acted as a lubricant. Similar studies were performed using pentanol films at 15 and 95% partial pressure delivered to the surface from the vapor phase [16].

B. P. Miller · N. D. Theodore · M. J. Brukman · J. Krim (✉)
Department of Physics, North Carolina State University,
Raleigh, NC 27695, USA
e-mail: jkrim@ncsu.edu

N. D. Theodore · K. J. Wahl
Chemistry Division, Code 6176, Naval Research Laboratory,
Washington, DC 20375, USA

M. J. Brukman
Department of Materials Science and Engineering, University
of Pennsylvania, Philadelphia, PA 19104, USA

The addition of pentanol vapor allowed a post and shuttle MEMS device, possessing a geometry comparable to a cylinder on flat, to run for longer than 100 million cycles at both partial pressures without failure so long as the device remained exposed to pentanol vapor [16]. Despite the success of these lubricants, an environment of vapor is needed to replenish the surface of the device for maintaining lubrication. However, this is impractical to implement especially for those devices that must be open to the surrounding environment to perform their intended task [17].

Tricresyl phosphate (TCP) is a well-known high temperature anti-oxidant additive to industrial oils and possesses a very low vapor pressure [18]. For hot ferrous bearing surfaces, vapor phase lubrication by TCP and similar organic molecules involves formation of a reaction film containing phosphate chemistries (see [19, 20] and references therein). Alternately, organic molecules like TCP can be condensed on bearing surfaces to provide liquid lubrication [19, 21]. By heating TCP, the vapor pressure is raised enough to condense a lubricating layer on exposed surfaces. The low vapor pressure under ambient conditions and ability to condense a lubricant film on a surface without significant line-of-sight limitations makes TCP a candidate of interest for MEMS lubrication to increase performance over chemically bound monolayer films [22–24].

The present study investigates the performance of TCP as a vapor phase-deposited liquid lubricant [14]. Specifically, the tribological properties of perfluorodecyltrichlorosilane (PFTS, chemically bound SAM) with and without TCP (mobile lubricant) present, using four techniques that span length scales ranging from nanometers to millimeters and mean Hertzian contact stresses up to 2 GPa. In the first method, a quartz crystal microbalance (QCM) was used to measure both the mass and interfacial viscosity of the lubricant adsorbed to the surface. Actual contacts, not only in MEMS but for the vast majority of surfaces, can be viewed as an open-faced sandwich where the liquid lubricant is not squeezed between two surfaces at all times. Thus, the lubricant is open to the environment and free to move around the surface. A QCM can log real-time measurements of interactions of vapor phase lubricants on surfaces [24–26], thus providing a realistic look into the surface mobility of a lubricant. Sliding contacts at three different scales were also examined using an AFM, a microtribometer, and a macroscopic tribometer: (1) a lateral force atomic force microscope (AFM) for a nanometer-scale model single-asperity contact at relatively high mean contact stresses (~ 1.8 GPa); (2) a reciprocating microtribometer for micrometer-scale measurements applying high mean contact stresses (~ 2 GPa); (3) and a macroscopic reciprocating tribometer for millimeter-scale tests at relatively low mean contact stresses (< 0.6 GPa). These experiments span contact pressures and length scales

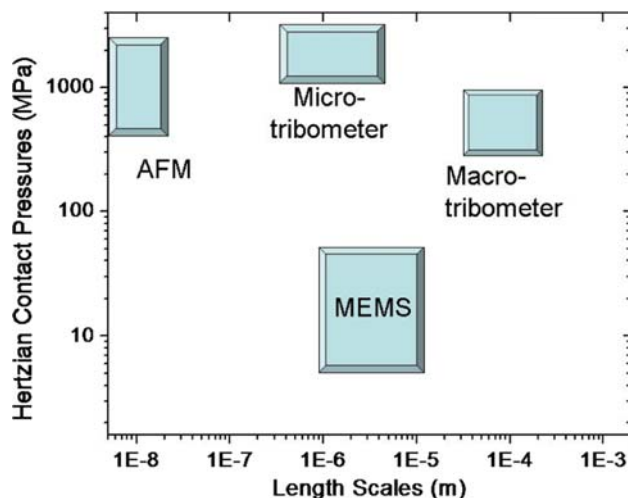


Fig. 1 Schematic showing contact pressures and length scales of the three tribometers compared to a MEMS device. Lubrication is seen over the entire range with the AFM, and at low pressures with the macrotribometer, but not at any pressures with the microtribometer

both above and below MEMS operational specifications (Fig. 1). The present article reports comparisons of lubrication performance of PFTS, with and without TCP, over a broad range of contact stresses and length scales.

2 Sample Preparation and Characterization

2.1 Perfluorodecyltrichlorosilane deposition procedure

Perfluorodecyltrichlorosilane layers were coated onto P-type, boron-doped, silicon (111) [28] substrates from standard solution techniques [29]. All samples were cleaned by first rinsing in water followed by a methanol rinse. To assure deposition uniformity, all the substrates were UV-ozone cleaned for 15 min and placed in subsequent baths of water, isopropanol (IPA), and trimethylpentane (TMP) for 5 min each. Following these surface preparation steps, the silicon samples were immersed for 2 h into a bath of PFTS/anhydrous TMP solution contained within a dry nitrogen environment; this procedure has been reported to provide a densely packed monolayer of PFTS on silicon oxide [29]. Next, the samples were placed into subsequent baths of TMP, IPA, and water for 5 min each to remove any unbonded silane chains. The same procedure was used to coat the aluminum and silicon dioxide electrodes used in QCM measurements.

2.2 Tricresylphosphate Deposition

Tricresylphosphate, obtained from the Naval Research Laboratory (Washington, DC), was deposited on PFTS-coated samples using a simple vacuum evaporation technique.

Samples were placed in a vacuum chamber directly above a tungsten wire crucible containing TCP. The vacuum chamber reached a base pressure 10^{-7} Torr with an ion pump without vaporization of the TCP. Deposition of TCP was performed by heating the crucible to over 100°C ; heating was necessary to release TCP into the vapor phase, since TCP has a low vapor pressure at room temperature [18]. During this process, the vacuum pressure was maintained at 10^{-6} Torr by using a turbomolecular pump and a liquid nitrogen trap to condense the TCP vapor to prevent contamination of the pump and its eventual release. A QCM was used to calibrate the deposition rate at a given substrate height so that the uptake of TCP onto the sample substrates was approximately the same for all deposition runs.

2.3 QCM

MEMS devices are currently fabricated from both silicon and aluminum [30], and so QCM uptake measurements were performed on four different commercially available substrates: (1) SiO_2 electrode, (2) PFTS on a SiO_2 electrode, (3) an Al electrode with a native oxide, and (4) PFTS-coated Al electrode possessing a native oxide. Aluminum was chosen for the electrode surface because in an ambient air environment it possesses a native surface oxide similar to that of silicon, allowing PFTS to bond similarly to the crystal surface [31]. The SiO_2 electrodes were commercially obtained as 5 MHz AT-cut quartz crystals with SiO_2 electrodes deposited onto an adhesive Ti interlayer [32]. The aluminum electrodes were fabricated by thermally evaporating titanium and aluminum layers in vacuo onto both sides of commercially available, blank 8 MHz AT-cut quartz crystals [33]. The titanium layer was 20 nm thick and acted as an adhesion layer for the 50 nm thick aluminum coating.

2.4 Characterization

To verify the deposition of the PFTS monolayer and the TCP lubricant layer, Fourier transform infrared (FTIR) and X-ray photoelectron spectroscopy (XPS) spectra were obtained from coated Si wafer surfaces. FTIR analyses were performed using a Thermo-Nicolet Magna 760 IR spectrometer with a liquid nitrogen-cooled, mercury–cadmium–telluride (MCT-B) detector; each spectrum was the sum of 128 scans taken with the resolution setting at 8 cm^{-1} (3.857 cm^{-1} data spacing), using a single bounce, germanium crystal, attenuated total reflection (ATR) accessory to probe the surface of the sample. XPS measurements (Thermo VG Scientific Escalab 220i-XL) were performed using a monochromatic Al $K\alpha$ source. Survey spectra (1.8 eV analyzer resolution, 1 eV point spacing) as well as high resolution scans (0.3 eV analyzer resolution,

0.1 eV point spacing) were taken at the primary energy regions for carbon (C 1s), silicon (Si 2p), oxygen (O 1s), fluorine (F 1s), and phosphorus (P 2p). Elemental spectrum fitting was completed using a commercially available software package [34] that fits the individual peaks with a convolution of Gaussian and Lorentzian line shapes after modeling the inelastic electron background with a linear combination of Shirley and polynomial functions.

Both XPS and FTIR confirmed that the deposition procedures produced surfaces containing the PFTS and TCP layers, respectively. The XPS survey spectrum of the PFTS coating on silicon and the TCP/PFTS layers on silicon confirmed the presence of all the expected surface species (silicon, carbon, oxygen, and fluorine) [35] except for phosphorus from TCP. Although peaks were evident in the P 2p region between 124 and 144 eV, these could not conclusively be identified as phosphorus since single crystal silicon substrates produce plasmon resonances that directly overlap at the same binding energy. High resolution scans of the C 1s region (Fig. 2), determined the presence of four peaks in both the PFTS coating and the combination TCP/PFTS layer on silicon. Two of these peaks are characteristic of surface carbon contaminants, and the other two are shifted to higher binding energies, typical of two unequivalent carbon–fluorine bonds, $-\text{CF}_2$ and $-\text{CF}_3$. These latter peaks confirmed the presence of carbon–fluorine bonding, found in PFTS, on the PFTS-coated silicon and the combination TCP/PFTS-layered silicon samples. No chlorine was observed in any of the XPS spectra, assuring that unreacted PFTS was not present.

FTIR spectroscopy of the PFTS coating (Fig. 3) on silicon using an uncoated silicon wafer as a reference revealed only the phonon absorption bands typical of uncoated silicon. Since the penetration depth of the evanescent wave in a single bounce Ge ATR accessory is approximately 300 nm, the signal from the lattice vibrations of the silicon substrate with its own native oxide greatly exceeded the signal from the single monolayer PFTS coating (~ 3 nm thick) that possessed Si–O and C–F bonding species [36]. Thus, the signal of the PFTS monolayer did not contain species that possessed a distinct, strong infrared absorption profile to distinguish it from the absorption of the silicon substrate. Absorption peaks from the underlying silicon substrate were also evident in the combined PFTS/TCP coating on silicon. However, the combination PFTS/TCP layer on silicon had numerous absorption bands from 500 to 1700 cm^{-1} . These peaks correspond directly to the expected absorption bands of liquid TCP [37]. Thus, FTIR spectroscopy verified TCP was in fact deposited during the evaporation procedure.

For completeness, a 300 MHz nuclear magnetic resonance (NMR) spectrometer was also used to determine the

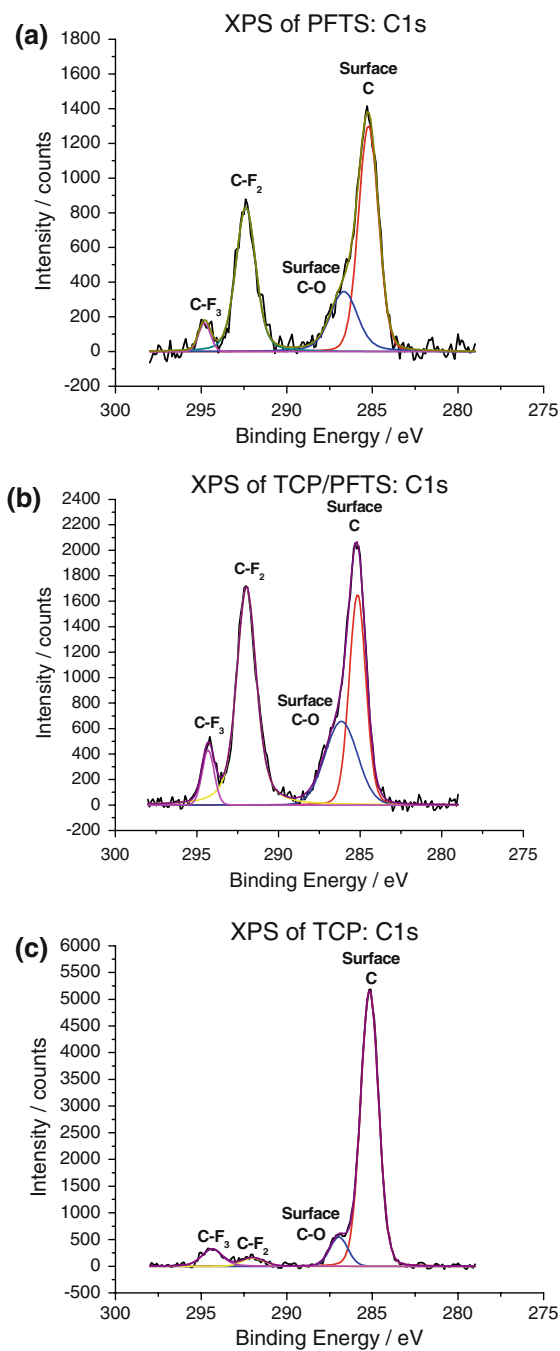


Fig. 2 Deconvoluted high-resolution XPS spectra of the C-1s region taken of (a) the bound PFTS layer on silicon and (b) the combined bound PFTS and mobile TCP coating confirmed the presence of the carbon-fluorine bonding, indicative of the C-F₂ and C-F₃ bonds present in PFTS. A deconvoluted XPS spectrum of the same region of (c) the mobile TCP layer deposited on silicon showed minimal C–F bonding

purity of the TCP used in these experiments. A sample was prepared by dissolving 1 μL of the (TCP) oil in 750 μL of deuterated chloroform (CDCl_3). ^1H solution state NMR experiments were recorded on an AVANCE-300 NMR

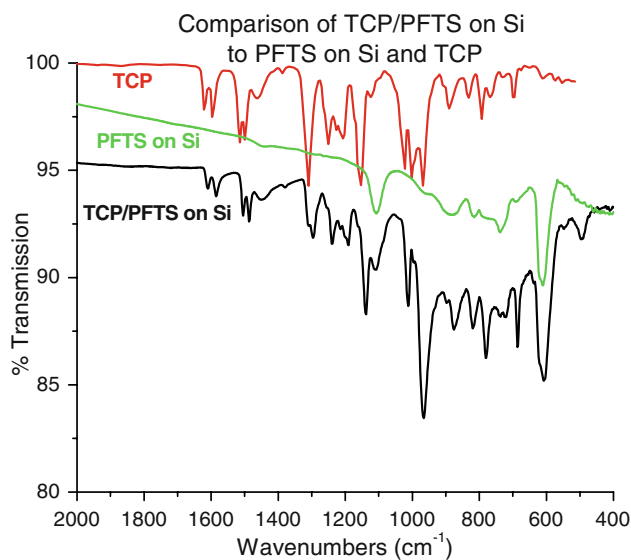


Fig. 3 Using an ATR accessory, FTIR spectra were taken of the combined bound PFTS/mobile TCP coating on silicon and PFTS on silicon. The PFTS on silicon showed absorption phonons from the underlying silicon substrate. Comparing these spectra to reference FTIR spectra of liquid TCP [36], confirmed that the spectrum of the bound PFTS/mobile TCP coating possessed absorption bands consistent with both TCP and silicon

spectrometer (Bruker, Billerica, MA) outfitted with a 5 mm z-pulsed field gradient (PFG) room temperature probe. A 1D spectrum was obtained by taking 128 scans with a 1.5 s recycle delay and 64,000 acquired data points. The spectrum was processed and analyzed with XWINNMR v3.5 (Bruker), and then compared to the estimated shifts seen from a structural NMR model of TCP, developed using ChemNMR, a commercially available software package. The only peaks present in the ^1H -NMR analysis were those expected to arise from TCP—split peaks around 2.25 ppm arising from the methyl group hydrogen atoms and split peaks around 7.15 ppm arising from the hydrogen atoms bound to the carbon phenyl ring. Thus, it was concluded that the TCP was pure, containing no other hydrogen-containing contaminants. Further analysis of the spectrum also revealed that the TCP contained a mixture of isomers (ortho-, meta-, and para-), with the meta-conformation as the predominant component, but a full description of that study is beyond the scope of this experiment.

3 Experimental Details

3.1 QCM Resonator

The QCM consists of a single crystal of quartz that oscillates in transverse shear mode with a high quality factor. The Sauerbrey equation [38] gives the mass uptake as a function of the change in resonant frequency of the QCM,

sensitive enough to measure adsorption of a tenth of a monolayer. Adsorption can also produce amplitude shifts due to frictional shear forces exerted on the surface electrode by the adsorbed film. These may arise from interfacial slippage of the layer, or alternatively viscoelastic effects within the film. For the case of interfacial slippage, characteristic slip times τ , and friction coefficients η , are determined by

$$\Delta Q^{-1} = -4\pi\tau\Delta f \quad \text{and} \quad \eta = \frac{\rho}{\tau} \quad (1)$$

where ΔQ^{-1} is the change in inverse quality factor, Δf is the change in frequency of the crystal, and ρ is the mass per unit area of the adsorbed film. The slip time is inversely proportional to the friction coefficient between the adsorbed layer and the substrate and corresponds to the average time for the film's velocity to fall to $1/e$ of its original value if the substrate is abruptly stopped. This deceleration is due to frictional forces between the substrate (bound SAM) and the adsorbed layer (mobile lubricant). The change in the inverse quality factor is proportional to the change in the inverse amplitude of the crystal, and that proportionality constant is calibrated through a known interaction of the crystal and nitrogen gas at varying pressures [27].

Once the crystals were coated with PFTS, they were placed in a vacuum chamber. Chamber pressure, amplitude, and frequency of the crystal were recorded simultaneously at 6-s intervals. Only additional adsorbing layers in the vapor phase were measured with the QCM. The slip time of TCP on PFTS/SiO₂, TCP on PFTS/Al with a native oxide, TCP on Al with a native oxide, and TCP on SiO₂ was determined.

3.2 Lateral Force AFM

Friction behavior of the PFTS and TCP/PFTS were measured by AFM (Asylum Research, Santa Barbara, CA) under ambient conditions. Olympus OMCL-RC800 rectangular (20 × 200 μm) SiN levers with pyramid silicon nitride tips (Si₃N₄, Olympus, Tokyo, Japan) having nominally a 20 nm tip radius and 0.05 N/m cantilever spring constants were used in as-received condition for experiments. Friction data as a function of applied load were obtained by scanning in contact mode while simultaneously ramping the normal force setpoint from positive (compressive) to negative (tensile) load until the tip separated from the surface. The adhesive force of the tip-sample junction was defined as the magnitude of the tensile force at pull-off while the lateral friction force was defined as the half-width of the friction force loop at each load. Normal and lateral forces were calibrated according to methods outlined in Refs. [39] and [40], respectively. The

normal force calibration [39] relies on the resonant frequency, quality factor, and geometry of the cantilever. The lateral force calibration [40] uses a commercially available grating with planar facets simplifying the calibration. Cantilever-tilt compensation was employed to reduce coupling with sample topography [41]. One PFTS-coated and one TCP/PFTS-coated Si wafer were tested at multiple points per wafer. Using 20 nm as the nominal tip radius, a Hertzian contact pressure of 1.8 GPa is calculated at the maximum load (~6 nN including adhesion).

Microscopic single-asperity interactions typically resulted in friction being a non-linear function of load—and sphere-on-SAM interactions can be particularly complex [42–44], so it was not entirely appropriate to use the metric “coefficient of friction” in this context. Instead we reported an *approximate* friction coefficient, defined as a linear fit to the data *in the positive loading regime only*. We justified this definition on the basis that (1) non-linear effects were more pronounced in the tensile regime, compromising the fitting process and (2) other sliding tests in this study were performed at positive load, so this usage best facilitated cross-technique comparison.

3.3 Micro- and Macroscale Reciprocating Tribometry

Reciprocating tribology tests were performed on microscopic and macroscopic scales using two different instruments to compare the friction properties of uncoated silicon, the bound PFTS layer, and the combination TCP/PFTS layers. Microscopic friction tests were completed using a scanning nanoindenter (Hysitron Triboscope) that utilizes a two-dimensional electrostatic driven force transducer and capacitive displacement sensing to simultaneously apply normal force while measuring lateral force during sliding. In these measurements, a 400 μN load was applied to a parabolic polished diamond counterface, ~8 μm radius, resulting in a mean Hertzian contact stress of ~2 GPa. The tip oscillated for 40 cycles along an 8 μm track at a rate of 4 μm/s.

Macroscopic sliding friction tests were performed on a homebuilt reciprocating tribometer with computer operated linear translation stages. Loads of 0.5 N were applied to a spherical sapphire counterface (radius 3.175 mm), resulting in mean Hertzian contact stresses of 0.35 GPa. Each sample oscillated against the sapphire counterface for 100 cycles along a 5 mm track at a rate of 1 mm/s in ambient laboratory conditions. Lateral force data were collected and averaged per sliding cycle and reported as friction coefficient (lateral/normal force). In addition, higher loads of 1 and 2 N were performed for the TCP/PFTS-coated silicon sample only.

4 Results

QCM data illustrated a sample run of TCP on one of each of the four substrates (Fig. 4). The graph displayed inverse quality factor of the QCM versus mass per unit area adsorbed to the surface, where the slope was proportional to the slip time. One set each for TCP on SiO₂ and TCP on PFTS/SiO₂ were performed for comparison to previous results of TCP on a SAM. TCP depositions on four different PFTS/Al samples and three different Al samples were also performed. Table 1 showed the average slip time and coverage for each of the experiments with the corresponding error. The uncertainty in the SiO₂ substrate measurements comes from the error in the best fit line, and

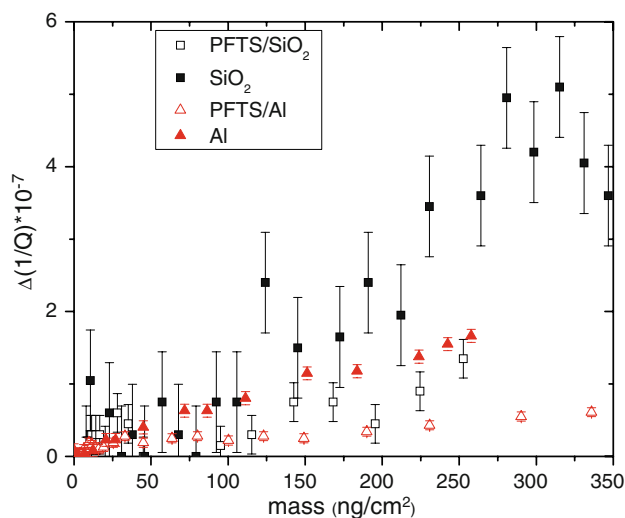


Fig. 4 QCM results of TCP on Al and Si and TCP on PFTS. The slope corresponds to the slip time, which is inversely proportional to the interfacial coefficient of friction. Both exhibit a non-zero slip time indicating mobility. TCP on uncoated silicon and aluminum shows a higher slip time than with the PFTS SAM

the uncertainty in the Al substrate measurements comes from the standard deviation of the multiple measurements. The QCM slip time results of TCP on SiO₂ and TCP on PFTS/SiO₂ agreed with previous measurements made with TCP on silicon with a native oxide and TCP on a SAM, respectively [21]. TCP on PFTS/SiO₂ and TCP on PFTS/Al should theoretically be equivalent and were, in fact, in acceptable agreement. Both showed less slip time than TCP on their respective sublayers (Table 1).

AFM friction testing was performed using a single tip to facilitate friction comparisons between samples and tests. First, six unloading friction experiments were performed on the PFTS-coated Si wafer and were repeated at another location on the wafer. Then, the sample was exchanged, and six unloading friction experiments were performed on the TCP/PFTS-coated Si wafer and were repeated at another location on the wafer. Finally, six unloading friction experiments were performed on a new location on the initial PFTS-coated wafer. Typical plots of frictional force versus normal load for one test (Fig. 5) showed that TCP increased adhesion (and therefore the total applied load [45]) compared to the PFTS layer alone. This increase of adhesion was attributed to capillary effects of liquid TCP layer in the tip-sample contact. The slope of the average linear fits corresponded to the approximate friction. Friction for the first two locations on the PFTS-coated samples was 0.30 ± 0.03 and on TCP/PFTS-coated wafers, 0.13 ± 0.01 . After returning to the initial PFTS samples, the friction coefficient was 0.20 ± 0.04 .

Microscopic friction experiments did not result in measurable differences between the friction of diamond against uncoated silicon and silicon coated with both PFTS and TCP layers; average friction coefficients were the same, ~ 0.08 , within the measurement error. The average friction coefficient for both samples decreased from ~ 0.09

Table 1 Summary of QCM experimental results for TCP adsorption on four different substrates

	SiO ₂		PFTS/SiO ₂		PFTS/Al		Al	
	Coverage	τ (ns)	Coverage	τ (ns)	Coverage	τ (ns)	Coverage	τ (ns)
TCP	3	0.90 ± 0.02	3	0.22 ± 0.02	4	0.13 ± 0.05	3	0.55 ± 0.15

The coverages are labeled in units of monolayers (ML)

Table 2 Overview of load, contact area, contact stress, and friction coefficient for the three different length scales

	AFM	Microtribometer	Macrotribometer
Load	6 nN	400 μ N	0.5 N
Hertzian contact area	~ 3 nm ²	~ 0.2 μ m ²	~ 1400 μ m ²
Hertzian contact pressure	1.8 GPa	1.8 GPa	0.35 GPa
μ on PFTS/Si	0.30 ± 0.05	0.08 ± 0.02	0.8 ± 0.1
μ on TCP/PFTS	0.12 ± 0.05	0.08 ± 0.02	0.16 ± 0.05

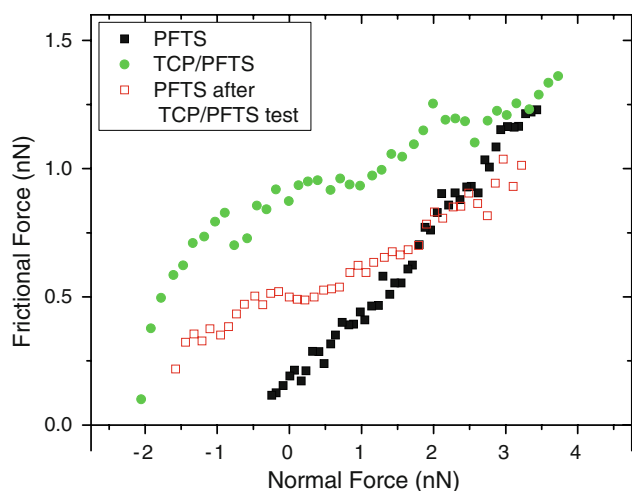


Fig. 5 Three characteristic AFM scans in lateral force mode show lower friction (as determined by the slope of the plots) with the TCP lubricant present. After testing TCP on PFTS, the frictional force of the PFTS layer by itself was measured again. The lower friction of the second PFTS test indicates that TCP transferred onto the AFM tip and continued to lubricate the PFTS-only specimen

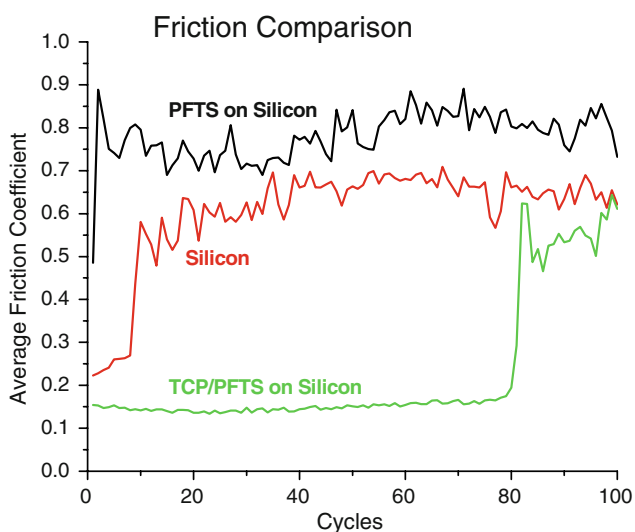


Fig. 6 Typical reciprocating macroscopic friction results from uncoated silicon, the bound PFTS layer on silicon, and the combined TCP/PFTS coating on silicon

to ~ 0.08 by cycle 10 and was stable for the remainder of the test.

Reciprocating macroscopic sliding experiments revealed repeatable differences among uncoated silicon, the PFTS layer, and the TCP/PFTS layer (Fig. 6). The average friction coefficient for uncoated silicon began at ~ 0.24 for eight cycles, followed by an immediate increase in friction coefficient to 0.55 – 0.65 for the remaining cycles occurring concurrently with the generation of significant wear debris. The average friction coefficient of the bound PFTS layer began high at 0.5 , and by cycle 2 was greater than 0.8 ,

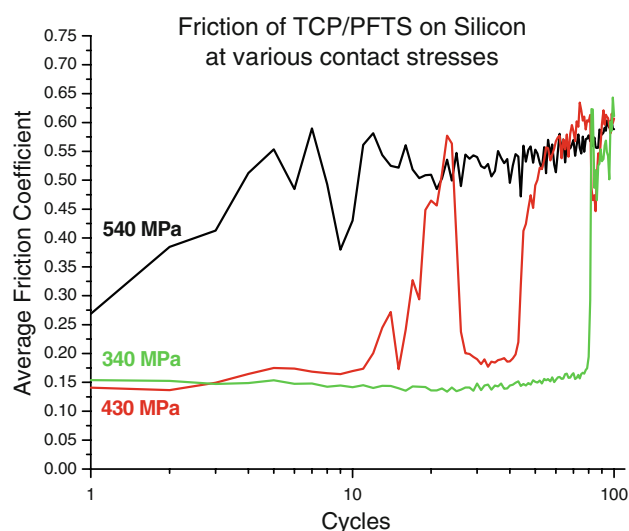


Fig. 7 Typical reciprocating macroscopic friction results from the combined TCP/PFTS coating on silicon as the average Hertzian contact stress is increased by raising the applied load from 0.5 N (340 MPa), to 1 N (430 MPa), and 2 N (540 MPa). The number of cycles at low friction (<0.2) decreases from about 80 cycles at 340 MPa to 15 cycles at 430 MPa to 0 cycles at 540 MPa. After possessing high friction for ~ 10 cycles, the friction during the 430 MPa test does recover to low friction for an additional 15 cycles before ultimately remaining at high friction. Note that the x-axis is on a log-scale

combined with the generation of visible debris on the track. However, the average friction coefficient for the TCP/PFTS was less than 0.2 for between 30 and 80 cycles before increasing to ~ 0.5 with the generation of visible wear debris.

To examine the frictional differences in the PFTS and TCP coating observed between microscopic and macroscopic testing, a separate macroscopic experiment was executed to explore the effect of increasing the mean Hertzian contact stress. Loads of 0.5 , 1 , and 2 N were applied to a sapphire counterface to produce mean Hertzian contact stresses of 0.35 , 0.44 , and 0.56 GPa, respectively (Fig. 7). With a 0.56 GPa mean contact stress, the average friction increased from 0.27 to 0.55 within 5 cycles. With a 0.44 GPa mean contact stress, the friction remained below 0.2 for 10 cycles, increased sharply to 0.55 during cycle 11, but then recovered to below 0.2 for 15 more cycles before incrementally increasing up to 0.60 . With a 0.35 GPa mean contact stress, the friction remained low for 80 cycles before incrementally increasing similarly to the previous test. Table 2 showed an overview of contact properties and the friction coefficient for the three different length scales.

5 Discussion

Adhesion and poor tribological properties lead to shortened MEMS device lifetimes, which limit their reliability and

utility. Currently, one way to minimize adhesion during the fabrication of MEMS is the addition of a SAM to the silicon surface [5]; the SAM produces a hydrophobic surface thereby preventing capillary forces from binding the moving parts. Since a SAM is already required for silicon MEMS fabrication, others have tried to use that same SAM to also reduce friction and wear, thereby increasing device lifetimes [46, 47]. However, the AFM and macrotribometer results showed that a PFTS SAM alone does not provide a low friction and wear contact. AFM experiments showed high friction coefficients of 0.30. Further macroscopic tests showed that PFTS had worse tribological behavior than uncoated silicon. These results are consistent with Hook's conclusion that a siloxane-coupled SAM cannot lubricate silicon MEMS since the applied mechanical energy in the contact exceeds the siloxane bonding energy of the SAM to the silicon surface [6].

The addition of a lubricant on top of the SAM can potentially improve the tribological performance by decreasing friction and wear over a longer period of time than without it. The AFM and macroscopic tribometry results support this claim. The PFTS layer had a high friction coefficient of 0.30, a *decrease* in the friction coefficient to 0.13 with the addition of TCP. However, the mechanism for friction reduction by the addition of TCP is not due to a decrease in adhesion. The x -intercepts from the AFM data (Fig. 5) showed that adhesion from the PFTS layer was approximately 0.5 nN, while the addition of TCP to PFTS *increased* adhesion to 2 nN. Since adhesion is a failure mechanism in a MEMS device, the ideal amount of TCP, which will lower the coefficient of friction but limit adhesion, has yet to be determined.

In the macroscale reciprocating tribometry tests on the PFTS layer on silicon, friction was high (>0.5) and significant silicon debris was generated quickly, similar to tests run on uncoated silicon. The addition of TCP, however, protected the underlying silicon substrate and reduced friction for the longest period of time of all the surface treatments examined. Thus, these macroscale tests confirmed that TCP is a lubricant lowering friction and wear. We note that the AFM used a silicon nitride tip, the microtribometer used a diamond counterface, and the macrotribometer used a sapphire counterface. If the TCP interacts differently with these materials, there may be additional contributions from the interface chemistry. This is beyond the scope of our paper.

Krim et al. have shown that favorable macroscopic tribological properties from a mobile lubricant corresponded to a non-zero slip time value on a QCM; poor macroscopic tribological properties occurred when QCM slip time values were zero [24, 25]. The QCM measurements showed that TCP possessed a non-zero slip time on PFTS, suggesting that TCP may in fact be mobile on the surface of PFTS. Lower friction was observed for AFM experiments

where PFTS was contacted after sliding the tip against a TCP/PFTS-coated sample. The reduced friction was attributed to TCP transferred to the AFM tip from the TCP/PFTS sample, which resulted in lower friction when that same tip was used on the previous PFTS surface.

In order to quantify the effect of mobility, a lubricant replenishment model posed by Brenner et al. [22] involving cyclic contact with a liquid lubricant was considered. This model assumes replenishment of the lubricant from lateral surface diffusion rather than vapor phase replenishment. The model parameters utilized the fraction of lubricant removed per stroke, frequency of oscillation, contact size, and surface diffusion coefficient of lubricant on a specific substrate to obtain a steady state concentration of lubricant at the center of contact. A similar "windshield wiper" model by Sawyer and Blanchet [23] involved lubricant replenishment from the vapor and does not take into account surface diffusion.

According to Brenner et al.'s [22] windshield wiper model, the steady-state center lubricant concentration is a function of three parameters: the contact area, frequency of oscillation, and diffusion coefficient. Using a $1 \mu\text{m}^2$ contact area and a simulated diffusion coefficient of $6.24 \times 10^{-5} \text{ cm}^2/\text{s}$ for TCP on a SAM, the steady-state center lubricant concentration of TCP on PFTS was 55%, assuming that 10% of the lubricant was removed per stroke and that the maximum oscillation frequency was 1000 Hz. The contact area is an integral part of this model, and as that value increases, the steady-state center concentration of lubricant will decrease to an amount insufficient for favorable tribological performance. The results supported this claim to a certain extent. When the loads during macroscopic tests were incrementally raised—thereby increasing the applied contact area and stress—while holding the oscillation frequency and diffusion coefficient constant, the protective and lubricating performance of the combined TCP/PFTS layer deteriorated, corresponding to a smaller steady-state center concentration of TCP as predicted by the model.

However, comparing the tribological results from the different length scales did not uniformly fit into the model. The theoretical model spans all dimensions with the only adjustable parameters being the diffusion coefficient, oscillation frequency, and contact size. For the present experiments, the only variables are oscillation frequency and contact size. If the oscillation frequency is also fixed, the time to replenish the lubricant at the center of the contact is determined by the contact radius. Based on this argument, the macroscale experiment should possess the worst tribological performance, with progressively smaller contacts performing better. So, according to the model, macroscopic tests that utilized a counterface almost 3 orders of magnitude greater than the microscopic tests and almost 5 orders of magnitude greater than the AFM should

have possessed the “worst” tribological properties since the lubricant would have less time to diffuse back into the entire contact area. This claim is supported by comparing the macroscale tests to the AFM results; although measurements on both instruments initially produce low friction, the larger contact in the macroscopic tests eventually produces high friction as the amount of TCP was not sufficient to maintain lubrication over time. However, macroscale tests showed better tribological properties of TCP on PFTS than microscale tests where friction was the same on TCP/PFTS and PFTS by itself.

One factor not considered in the above discussion is contact stress. The average contact stress of the microtribometry tests was 2 GPa, whereas the mean contact stress for the macrotribometry tests was only 0.34 GPa. In fact, the friction measurements of TCP on PFTS from millimeter, micrometer, and nanometer dimensions produced results sorted by contact stress. However, similar maximum mean contact stresses in the AFM and microtribometer tests (1.8 GPa in the AFM compared to 2 GPa in the microtribometer) but widely different friction response suggests that both the contact stress and the corresponding contact size should be considered when characterizing the tribological properties of lubricants at different length scales. These results showed that the bound PFTS and mobile TCP coatings may not be effective in a high contact stress environment, and that length scale (e.g., the contact area) should be taken into account.

Additionally, QCM tests measured a higher slip time for only TCP compared to TCP/PFTS on aluminum and silicon oxide. Studies have shown that the slip time is proportional to the diffusion coefficient indicating a higher diffusion coefficient [48]. Thus, according to the model, TCP, having a higher slip time without the presence of PFTS, would possess the same steady-state center concentrations (as modeled by Brenner) even at higher oscillation frequencies, improving the frequency range that TCP will successfully lubricate.

6 Summary

The main issues limiting reliability of silicon MEMS devices result from poor tribological performance and adhesion. Applying a SAM to the silicon can prevent stiction during MEMS fabrication but does not provide a lasting low friction interface [6]. The present results show that over a large range of contact sizes and stresses, the tribological performance of the PFTS layer was inadequate, resulting in high friction. In general, the results showed that the addition of TCP to PFTS reduced friction and increased sliding lifetime. The frictional differences measured among the scales (AFM, microtribometer, and macrotribometer) were

sorted by contact stress and contact size, where high stresses and larger contacts reduced lubricant performance. QCM results showed non-zero slip time of TCP on PFTS, suggesting TCP mobility on PFTS. Overall, at all length scales, the addition of TCP improved tribological properties by either reducing friction or increasing sliding lifetimes.

Acknowledgments This work has been funded by the AFOSR Extreme Friction MURI # FA9550-04-1-0381, and the basic research program of the Naval Research Laboratory. The authors would like to thank Daniel Barlow, Dmitri Petrovykh, and John Kulp for characterization assistance using FTIR, XPS, and NMR, respectively, as well as Adam Hook, Michael Dugger, and Colin Baker for useful discussions.

References

- Kim, S.H., Asay, D.B., Dugger, M.T.: Nanotribology and MEMS. *Nanotoday* **2**(5), 22–29 (2007)
- Komvopoulos, K.: Adhesion and friction forces in microelectromechanical systems: mechanisms, measurement, surface modification techniques, and adhesion theory. *J. Adhesion Sci. Technol.* **17**, 477–517 (2003)
- Timpe, S.J., Komvopoulos, K.: An experimental study of sidewall adhesion in microelectromechanical systems. *J. Microelectromech. Syst.* **14**(6), 1356–1363 (2005)
- Mastrangelo, C.H.: Adhesion related failure mechanisms in micromechanical devices. *Tribol. Lett.* **3**, 223–238 (1997)
- Maboudian, R., Ashurst, W.R., Carraro, C.: Tribological challenges in micromechanical systems. *Tribol. Lett.* **12**, 95–100 (2002)
- Hook, D.A., Dugger, M.T., Krim, J.: Monolayer degradation in MEMS friction devices. *J. Appl. Phys.* **104**, 034303 (2008)
- Eapen, K.C., Patton, S.T., Zabinski, J.S.: Lubrication of MEMS using bound and mobile phases of Fomblin Zdol. *Tribol. Lett.* **12**, 35–41 (2002)
- Ren, S.L., Yang, D.R., Zhao, Y.P.: Micro- and macro-tribological study on a self-assembled dual-layer film. *Langmuir* **19**, 2763–2767 (2003)
- Satyanarayana, N., Sinha, S.K.: Tribology of PFPE overcoated self-assembled monolayers deposited on Si surface. *J. Phys. D Appl. Phys.* **38**, 3512–3522 (2005)
- Satyanarayana, N., Sinha, S.K., Ong, B.H.: Tribology of a novel UHMWPE/PFPE dual-film coated onto Si surface. *Sens. Actuators A* **128**, 98–108 (2006)
- Ma, J.Q., Pang, D.J., Mo, Y.F., Bai, M.W.: Preparation and tribological properties of multiply-alkylated cyclopentane (MAC)-octadecyltrichlorosilane (OTS) double-layer film on silicon. *Wear* **263**, 1000–1007 (2007)
- Yu, B., Qian, L., Yu, J., Zhou, Z.: Effects of tail group and chain length on the tribological behaviors of self-assembled dual-layer films in atmosphere and in vacuum. *Tribol. Lett.* **34**, 1–10 (2009)
- Maboudian, R., Howe, R.T.: Critical review: adhesion in surface micromechanical structures. *J. Vac. Sci. Technol. B* **15**, 1–20 (1997)
- Krim, J., Abdelmaksoud, M.: Nanotribology of vapor-phase lubricants. In: Bhushan, B. (ed.) *Tribology Issues and Opportunities in MEMS*, pp. 273–284. Klumer Academic, Dordrecht (1998)
- Patton, S.T., Cowan, W.D., Eapen, K.C., Zabinski, J.S.: Effect of surface chemistry on the tribological performance of a MEMS electrostatic lateral output. *Tribol. Lett.* **9**, 199–209 (2001)
- Asay, D.B., Dugger, M.T., Kim, S.H.: In situ vapor-phase lubrication of MEMS. *Tribol. Lett.* **29**, 67–74 (2008)

17. McComas, D.J., Miller, G.P., Mitchell, J.N., Pope, S.E., Valek, P.W.: Space applications of microelectromechanical systems: Southwest Research Institute vacuum microprobe facility and initial vacuum test results. *Rev. Sci. Instrum.* **74**, 3874–3878 (2003)
18. Faut, O.D., Wheeler, D.: On the mechanism of lubrication by tricresylphosphate (TCP)—the coefficient of friction as a function of temperature for TCP on M-50 steel. *ASLE Trans.* **26**, 344–350 (1983)
19. Forster, N.H., Trivedi, H.K.: Rolling contact testing of vapor phase lubricants—Part I: material evaluation. *Tribol. Trans.* **40**, 421–428 (1997)
20. Forster, N.H.: Rolling contact testing of vapor phase lubricants—Part III: surface analysis. *Tribol. Trans.* **42**, 1–9 (1999)
21. Klaus, E.E., Duda, J.L.: Vapor Phase Lubrication Developments for Engines. SAE Pub. No. SP-256, pp. 541–550. SAE, Warrendale, PA (1991)
22. Brenner, D.W., Irving, D.L., Kingon, A.I., Krim, J.: Multiscale analysis of liquid lubrication trends from industrial machines to micro-electro-mechanical systems. *Langmuir* **23**, 9253–9257 (2007)
23. Sawyer, W.G., Blanchet, T.A.: Vapor-phase lubrication in combined rolling and sliding contacts: modeling and experimentation. *J. Tribol.* **123**, 572–581 (2001)
24. Abdelmaksoud, M., Bender, J., Krim, J.: Bridging the gap between macro- and nanotribology: a quartz crystal microbalance study of tricresylphosphate uptake on metal and oxide surfaces. *Phys. Rev. Lett.* **92**, 1–4, art. no 176101 (2004)
25. Abdelmaksoud, M., Bender, J., Krim, J.: Nanotribology of a vapor-phase lubricant: a quartz crystal microbalance study of tricresylphosphate (TCP) uptake on iron and chromium. *Tribol. Lett.* **13**, 179–186 (2002)
26. Neeyakorn, W., Varma, M., Jaye, C., Burnette, J.E., Lee, S.M., Nemanich, R.J., Grant, C.S., Krim, J.: Dynamics of vapor-phase organophosphates on silicon and OTS. *Tribol. Lett.* **27**, 269–276 (2007)
27. Krim, J., Widom, A.: Damping of a crystal-oscillator by an adsorbed monolayer and its relation to interfacial viscosity. *Phys. Rev. B* **38**, 12184–12189 (1988)
28. Wafer World. West Palm Beach, FL 33407. Part number: 1194
29. Srinivasan, U., Houston, M.R., Howe, R.T., Maboudian, R.: Alkyltrichlorosilane-based self-assembled monolayer films for stiction reduction in silicon micromachines. *J. Microelectromech. Syst.* **7**, 252–260 (1998)
30. Hornbeck, L.J.: The DMD (TM) projection display chip: a MEMS-based technology. *MRS Bull.* **26**, 325–327 (2001)
31. Devaprakasam, D., Sampath, S., Biswas, S.K.: Thermal stability of perfluoroalkyl silane self-assembled on a polycrystalline aluminum surface. *Langmuir* **20**, 1329–1334 (2004)
32. Maxtek, Inc. (part of Inficon). East Syracuse, NY 13057. Part number: 149277-1
33. Colorado Crystal Corporation. Loveland, CO 80537. Part number: CCAT1BK-1004-000
34. Hesse, R., Chassé, T., Szargan, R.: Peak shape analysis of core level photoelectron spectra using UNIFIT for WINDOWS. *Fresenius' J. Anal. Chem.* **365**, 48–54 (1999)
35. Wheeler, D.R., Faut, O.D.: The adsorption and thermal decomposition of tricresylphosphate (TCP) on iron and gold. *Appl. Surf. Sci.* **18**, 106–122 (1984)
36. Boyle, R.: FT-IR Measurement of Interstitial Oxygen and Substitutional Carbon in Silicon Wafers. Application Note #50640, Thermo Fisher Scientific, Madison, WI (2008)
37. Bertrand, P.A.: Reactions of tricresyl phosphate with bearing materials. *Tribol. Lett.* **3**, 367–377 (1997)
38. Sauerbrey, G.: *Z. Phys.* **155**, 206–222 (1959)
39. Sader, J.E., Chon, J.W.M., Mulvaney, P.: Calibration of rectangular atomic force microscope cantilevers. *Rev. Sci. Instrum.* **70**, 3967–3969 (1999)
40. Varenberg, M., Etsion, I., Halperin, G.: An improved wedge calibration method for lateral force in atomic force microscopy. *Rev. Sci. Instrum.* **74**, 3362–3367 (2003)
41. Cannara, R.J., Brukman, M.J., Carpick, R.W.: Cantilever tilt compensation for variable-load atomic force microscopy. *Rev. Sci. Instrum.* **76**, 053706 (2005)
42. Brukman, M.J., Marco, G.O., Dunbar, T.D., Boardman, L.D., Carpick, R.W.: Nanotribological properties of alkanephosphonic acid self-assembled monolayers on aluminum oxide: effects of fluorination and substrate crystallinity. *Langmuir* **22**, 3988–3998 (2006)
43. Chandross, M., Lorenz, C.D., Stevens, M.J., Grest, G.S.: Simulations of nanotribology with realistic probe tip models. *Langmuir* **24**, 1240–1246 (2008)
44. Flater, E.E., Ashurst, W.R., Carpick, R.W.: Nanotribology of octadecyltrichlorosilane monolayers and silicon: self-mated versus unmated interfaces and local packing density effects. *Langmuir* **23**, 9242–9252 (2007)
45. Carpick, R.W., Agrait, N., Ogletree, D.F., Salmeron, M.: Variation of the interfacial shear strength and adhesion of a nanometer-sized contact. *Langmuir* **12**, 3334–3340 (1996)
46. Ren, S., Yang, S., Zhao, Y., Zhou, J., Xu, T., Liu, W.: Friction and wear studies of octadecyltrichlorosilane SAM on silicon. *Tribol. Lett.* **13**, 233–239 (2002)
47. Singh, R.A., Yoon, E., Han, H., Kong, H.: Friction behaviours of chemical vapor deposited self-assembled monolayers on silicon wafer. *Wear* **262**, 130–137 (2007)
48. Miller, B.P.: Diffusion of physisorbed layers and their connection to MEMS effectiveness. PhD dissertation